[3] T. W. Graham and A. G. Sabelnikov, "How much is enough: Real-time detection and identification of biological weapon agents," *J. Homeland Sec. Emerg. Manage.*, vol. 1, no. 3, p. Article 303, Jun. 2004.

[4] G. M. Murrar and G. E. Southard, "Sensors for chemical weapons detection," *IEEE Instrum. Meas. Mag.*, vol. 5, no. 4, pp. 12–21, Dec. 2002.

[5] L. Henesey, F. Wernstedt, and P. Davidsson, "A market-based approach to container port terminal management," in *Proc. 15th Eur. Conf. Artif. Intell.*, Lyon, France, Jul. 2002, pp. 79–84.

[6] M. Rebollo, V. Julian, C. Carrascosa, and V. Botti, "A multi-agent system for the automation of a port container terminal," in *Proc. Autonomous Agents 2000 Workshop on Agents in Industry*, Barcelona, Spain, 2000, pp. 1–6.

[7] A. Erera, K.-H. Kwek, N. Goswami, C. White, and H. Zhang, "Cost of security for sea cargo transport." [Online]. Available: http://www2.isye.gatech.edu/setra/reports/Security_Cost_Report_May2003.pdf.

[8] L. M. Wein, A. H. Wilkins, M. Baveja, and S. E. Flynn, "Preventing the importation of illicit nuclear materials in shipping containers," *Risk Anal.*, vol. 26, no. 5, pp. 1377–1393, 2006.

[9] B. M. Lewis, A. L. Erera, and C. C. White, "Optimization approaches for efficient container security operations at transshipment seaports," *Transport. Res. Rec.*, vol. 1822, pp. 1–8, 2003.

[10] P. D. Stroud and K. J. Saeger, "Enumeration of increasing Boolean expressions and alternative digraph implementations for diagnostic applications," in *Proc. Comput., Commun., Technol.*, 2003, pp. 328–333.

[11] D. Madigan, S. Mittal, and F. Roberts, "Sequential decision making algorithms for port of entry inspection: Overcoming computational challenges," in *Proc. IEEE Int. Conf. on Intelligence and Security Informatics (ISI-2007)*, May 23–24, 2007, pp. 1–7.

[12] H. L. Lee, "On the optimality of a simplified multicharacteristic component inspection model," *IIE Trans.*, vol. 20, no. 4, pp. 392–398, 1988.

[13] A. Raouf, J. K. Jain, and P. T. Sathe, "A cost-minimization model for multicharacteristic component inspection," *IIE Trans.*, vol. 15, no. 3, pp. 187–194, 1983.

[14] S. O. Duffuaa and A. Raouf, "An optimal sequence in multicharacteristic inspection," *J. Optim. Theory Appl.*, vol. 67, no. 1, pp. 79–87, 1990.

[15] L. A. Cox , Jr, Y. Qiu, and W. Kuehner, "Heuristic least-cost computation of discrete classification functions with uncertain argument values," *Ann. Oper. Res.*, vol. 21, pp. 1–21, 1989.

[16] J. C. Bioch and T. Ibaraki, "Complexity of identification and dualization of positive Boolean functions," *Inform. Comput.*, vol. 123, pp. 51–75, 1995.

[17] M. Chang, W. Shi, and W. K. Fuchs, "Optimal diagnosis procedures for k-out-of-n structures," *IEEE Trans. Comput.*, vol. 39, pp. 559–564, 1990.

[18] E. Boros and T. Unluyurt, "Diagnosing double regular systems," *Ann. Math. Artif. Intell.*, vol. 26, pp. 171–191, 1999.

[19] L. M. Wein, Y. Liu, Z. Cao, and S. E. Flynn, "The optimal spatiotemporal deployment of radiation portal monitors can improve nuclear detection at overseas ports," *Sci. Global Security*, vol. 15, pp. 211–233, 2007.

[20] E. A. Elsayed, C. M. Young, M. Xie, H. Zhang, and Y. Zhu, "Port-of-entry inspection: Sensor deployment policy optimization," *IEEE Trans. Autom. Sci. Eng.*, vol. 6, pp. 265–276, Apr. 2009.

[21] M. N. Azaiez and V. M. Bier, "Optimal resource allocation for security in reliability systems," *Eur. J. Oper. Res.*, vol. 181, pp. 773–786, 2007.

[22] Y. Ben-Dov, "Optimal testing procedures for special structures of coherent systems," *Manage. Sci.*, vol. 27, no. 12, pp. 1410–1420, 1981.

[23] R. W. Butterworth, "Some reliability fault-testing models," *Oper. Res.*, vol. 20, pp. 335–343, 1972.

[24] L. Cox, S. Chiu, and X. Sun, "Least-cost failure diagnosis in uncertain reliability systems," *Rel. Eng. Syst. Safety*, vol. 54, pp. 203–216, 1996.

[25] J. Halpern, "Fault-testing of a k-out-n system," *Oper. Res.*, vol. 22, pp. 1267–1271, 1974.

[26] J. Halpern, "A sequential testing procedure for a system's state identification," *IEEE Trans. Reliab.*, vol. R-23, no. 4, pp. 267–272, 1974.

[27] J. Halpern, "The sequential covering problem under uncertainty," *INFOR*, vol. 15, pp. 76–93, 1977.

[28] L. Devroye, *Non-uniform Random Variate Generation*. New York: Springer-Verlag, 1986, ch. 2, p. 28.

[29] J. K. Kihlberg, J. H. Herson, and W. E. Schotz, "Square root transformation revisited," *Appl. Statist.*, vol. 21, pp. 76–81, 1972.

[30] I. D. Jupp, P. T. Durrant, D. Ramsden, T. Carte, G. Dermody, I. B. Pleasants, and D. Burrows, "The non-invasive inspection of baggage using coherent X-ray scattering," *IEEE Trans. Nucl. Sci.*, vol. 47, pp. 1987–1994, Dec. 2000.

[31] , H. Eschenauer, J. Koski, and A. Osyczka, Eds., *Multicriteria Design Optimization*. Berlin, Germany: Springer-Verlag, 1990.

[32] R. S. Statnikov and J. B. Matusov, *Multicriteria Optimization and Engineering*. New York: Chapman & Hall, 1995.

[33] M. Fonseca and P. J. Fleming, "Multiobjective optimization and multiple constraint handling with evolutionary algorithms—Part I: Unified formulation," *IEEE Trans. Syst., Man, Cybern. A*, vol. 28, no. 1, pp. 26–37, 1998.

[34] M. Fonseca and P. J. Fleming, "Multiobjective optimization and multiple constraint handling with evolutionary algorithms—Part II: Application example," *IEEE Trans. Syst., Man, Cybern. A*, vol. 28, no. 1, pp. 38–47, 1998.

[35] Y. W. Leung and Y. Wang, "Multiobjective programming using uniform design and genetic algorithm," *IEEE Trans. Syst., Man, Cybern. C*, vol. 30, no. 3, pp. 293–304, 2000.

[36] M. Mitchell, *An Introduction to Genetic Algorithms*. Cambridge, MA: MIT Press, 1996.

[37] *Genetic Algorithm and Direct Search Toolbox™ 2 User's Guide*. Natick, MA: MathWorks, Inc., 2008.

Surface Patch Reconstruction From "One-Dimensional" Tactile Data

Yan-Bin Jia and Jiang Tian

Abstract—This paper studies the reconstruction of unknown curved surfaces through finger tracking. A patch can be generated from tactile data points along three concurrent surface curves under the Darboux frame estimated at the curve intersection point. Surface fitting while minimizing the total (absolute) Gaussian curvature effectively prevents unnecessary folds otherwise expected to result from the use of such "1-D" data. The implementation involves a two-axis joystick sensor, a three-fingered 4-DOF BarrettHand, and a 4-DOF Adept SCARA robot. Experiments have demonstrated good accuracy of reconstruction.

Index Terms—Contour tracking, shape reconstruction, surface fitting, total Gaussian curvature, touch sensing.

I. INTRODUCTION

Objects with curved shapes are ubiquitous in our lives, from small ones such as pens, computer mice, or teapots to big ones such as chairs, cars, or airplanes. The differentiability of a curved shape allows smooth integration of kinematics, dynamics, and control, which paves the way for skillful maneuvers by a robot hand [13].

The human hand can often feel an unknown shape by moving the fingers across its surface. A robot hand with touch sensing capability should be able to accomplish the same. The difference is that the human hand can control its motions smoothly (and freely) based on its sensations. In addition, the number and density of tactels on a finger or the palm of the human hand far exceed what can be fabricated into a tactile array sensor with which a robot hand is equipped.

Shape reconstruction has traditionally been carried out by a vision system or a laser scanner. For example, many off-the-shelf laser scanners can produce global shapes efficiently with high accuracies (in hundredths of a millimeter). However, vision and scanner systems suffer from occlusions due to viewing angles and shape concavities. In a task like dexterous manipulation that requires close contact, the robot hand needs to determine the (local) shape in touch before or amid a maneuver, but the target area is usually occluded from the camera (by the hand itself). In addition, the lighting conditions may change during a task, and the background information may be distracting and difficult to filter out. The quality of range data also deteriorates in the presence of a motion. Although vision has been integrated with tactile sensing in tasks like object recognition and grasping [1], its usage is rather limited in other tasks such as in-hand dexterous manipulation [38] and perception of fine surface features [24].

Touch sensing is often the modality of choice in a task that heavily depends on the local shapes of the object surrounding the finger contacts. Tactile data usually reveal enough about the local geometry of contact for the execution of the task [4], since for them, occlusion ceases to be an issue.

In this paper, we demonstrate that the local shape of a three-dimensional (3-D) object in contact can be estimated using "one-dimensional" (1-D) data, namely, points sampled along three concurrent curves on the surface. The reconstruction is carried out by first recovering the differential geometry at the curve intersection point and then by fitting over the data under some geometric constraint. Compared to mechanical probing, curve tracking is a much more efficient physical operation to perform.

Besides the use of minimal data, the proposed reconstruction scheme has the ability to model general curved shapes (at least locally) with no constraints on the principal curvatures. Existing tactile recognition and reconstruction methods primarily use 2-D array data [1], [2], [18] with longer acquisition time. Some of them either assume special geometry (e.g., planar, polyhedral, spherical, cylindrical, or generalized cylindrical) of the objects [18] or show experimental results only on such objects [43].

Our experimental setup is a two-axis joystick sensor attached to one finger of a 4-DOF BarrettHand, which is mounted on a 4-DOF Adept Cobra 600 manipulator. The Adept's high positional accuracies[1] allow us to simplify tracking control and focus on reconstruction over contour data. Good accuracies of reconstructed patches have been demonstrated experimentally by matching against mesh models of the same objects generated by a commercial 3-D scanner.

Besides grasping and dexterous manipulation, our tactile reconstruction method may be applicable in robot-assisted surgery where details of a defected bone are sometimes occluded from a camera. Other potential applications include robotic planetary exploration, modeling of manufactured parts, and even rock climbing. For instance, in a situation like cave exploration where a camera will not work well due to occlusions and dim lighting conditions, a robot may have to rely on touching and fumbling to feel the rocks around in its search for a path.

In Section III, we describe a canonical polynomial representation of a surface patch under the Darboux frame estimated at the intersection point of three data curves. Each curve is generated by tracking the surface with a joystick sensor while constrained in a separate plane. The idea is to reduce the physical component of 3-D reconstruction into multiple subproblems of 2-D contour tracking.

Section IV describes a surface fitting algorithm that takes the insufficient "1-D" tracking data and simultaneously minimizes the total absolute Gaussian curvature of the surface function. Section V discusses implementation issues and presents some reconstruction results. Finally,

Section VI discusses various aspects of the presented research and outlines the future effort.

II. RELATED WORK

This paper is about reconstruction of curved surfaces. The physical operation involves tracking with a touch sensor under hybrid control. A surface patch is obtained through fitting over the tracking data in a local frame that is set up via estimation of principal curvatures.

A. Contour Tracking

Hybrid position/force control, originally proposed by Raibert and Craig [42], has been a favorable implementation strategy for tracking. Independent position control and force control are applied along unconstrained and constrained directions, respectively. Khatib and Burdick [31] later incorporated the dynamic coupling effects of motion and force equations at each robot joint.

De Schutter and Van Brussel [15] investigated tracking of unknown 2-D contours with constant tangential speed and contact force. Demey *et al.* [14] employed a 6 degrees-of-freedom (DOF) force/torque (F/T) sensor to carry out tracking of 2-D contours with known models. Oscillations during tracking were compensated by Jatta *et al.* [26] through the addition of a normal velocity feedback loop. Without resorting to direct force control, Lange and Hirzinger [32] enhanced second round contour tracking by transforming readings from an external F/T sensor into desired locations for position control.

In practice, contours (and motion constraints) are often unknown, and can be guided by a vision system [3]. Xiao *et al.* [51] also used visual guidance fused with hybrid position/force control to follow a trajectory (specified in the image plane) on an unknown surface.

B. Curvature Estimation

Methods for obtaining principal curvatures from normal curvature estimates have been developed mostly over dense range data [11], [23], [47] to better deal with noise. They are not robust when applied to sparse tactile data.

Analytical methods [21], [45] for curvature estimation generally fit over range data in the neighborhood of some point of interest and then obtain the first and second fundamental forms through differentiation. In [20], the principal curvatures were obtained through an initial fitting followed by an iterative minimization over their variations, as well as the variations along the surface normal and principal directions. Discrete methods based on surface triangulation such as in [33] may suffer from large estimation errors due to loss of differentiability.

Fearing and Binford [19] employed a cylindrical tactile fingertip mounted on the Stanford/JPL hand to estimate principal curvatures on quadric surfaces. In [30], curvatures, torsions, and their derivatives were estimated at points on one or two curves embedded on a surface, and based on them, differential invariants were derived for recognition of special surfaces. Smoothing of a planar curve was achieved through curvature minimization in order to extract segments at multiple scales for recognition [16]. In [25], two rounds of local fitting over tactile data from a 2-D shape were applied to robustly estimate the curvature and its derivative with respect to arc length.

C. Shape Reconstruction

In computer vision, shapes are often represented implicitly using polynomials generated via least-squares fitting, mostly for the convenience of operations such as inside-outside testing, handling of noisy data, and computation of algebraic invariants for recognition [28]. Polynomials of even degrees are often used because their level sets are bounded, which is not the case for those of odd degrees [48]. Typically, a subclass of quartic polynomials is chosen and constraints

---

[1]0.02 mm in the x- and y-directions and 0.01 mm in the z-direction.

are incorporated into least-squares formulations [29], [46]. Multiple level sets may also be used to further constrain the fitting, as in the case of the $3L$ algorithm [5].

Shape reconstruction using touch sensors has been studied by a number of researchers in robotics. Montana [37] derived a set of differential equations governing contact kinematics and employed it to estimate the local curvature of an unknown object under rolling contact with the robot finger. His contact equations were later used in [12] for measuring principal curvatures and directions from tactile data for motion control under rolling and sliding contacts. Bicchi *et al.* [4] considered shape reconstruction of an unknown object during rolling manipulation by a dexterous gripper.

Allen and Michelman [2] employed a Utah-MIT hand to obtain sparse contact points around an object and then fit a superquadric surface to the data as the reconstructed shape. An active sensing strategy was proposed in [10] to reconstruct local shape as a second order polynomial over dense tactile array data and servo the robot motion based on such shape information. The work by Charlebois *et al.* [9] involved the use of a B-spline over position, as well as normal data. Ellis and Qin [17] studied shape recovery from the strain on a tactile sensor, formulating it as an optimization problem solvable by the Levenberg–Marquardt method. Moll and Erdmann [36] showed how to simultaneously estimate the shape and motion of an unknown convex object from tactile readings on multiple manipulating palms under frictionless contact.

Over dense 3-D point data, triangulation [6], [34] is effective in constructing a model that reflects the correct topology of the original object.

III. PATCH ON A SURFACE

In the remainder of the paper, we will demonstrate that surface patches can be reconstructed rather accurately from seemingly insufficient "1-D" data generated by finger tracking. We employ the tracking subroutine from [35], which can reliably generate high accuracy[2] 2-D contours.

A. Approximation in a Local Frame

We begin with some geometric basics that are needed for the task. Let p be a point of interest on a curved object. We would like to obtain some description of a local area, or a "patch," surrounding p on the object's surface. The following assumption is made.[3]

A one-to-one correspondence exists between the patch to be reconstructed and its projection on the tangent plane at p.

Under the assumption, we need only consider a Monge patch which has the form $\boldsymbol{\sigma}(x, y) = (x, y, z(x, y))$. Here, we let z be approximated by a polynomial $\sum_{0 \le i+j \le d} a_{ij} x^i y^j$, where the degree d is chosen to reflect the geometric variation in the target area.

Set up a local frame at p with its xy-plane aligned with the tangent plane to the surface at the point, and its z axis aligned with the outward normal $\boldsymbol{n}$. Any plane through p that is normal to the tangent plane will intersect the surface $\boldsymbol{\sigma}$ at a curve (at least locally). Its curvature κ_n at p is the *normal curvature* of $\boldsymbol{\sigma}$ in the tangent direction where the two planes intersect. It is well-known that κ_n achieves its minimum and maximum (in case they are not equal) in two orthogonal tangent directions that are called the *principal directions*, denoted by $\boldsymbol{d}_1$ and $\boldsymbol{d}_2$, at p. These two extrema are the *principal curvatures* κ_1 and κ_2 in $\boldsymbol{d}_1$
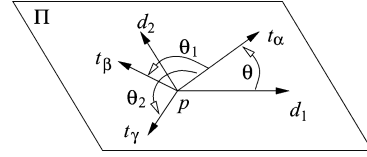
Fig. 1. Tangent plane at the reference point p of sampling.

and $\boldsymbol{d}_2$, respectively. The product $K = \kappa_1 \kappa_2$ is the *Gaussian* curvature at p.

The normal $\boldsymbol{n}$ and the principal directions $\boldsymbol{d}_1$ and $\boldsymbol{d}_2$ form the *Darboux frame* under which the local surface patch is shown [27] to take the form

$$z(x, y) = \frac{1}{2}(\kappa_1 x^2 + \kappa_2 y^2) + \sum_{3 \le i+j \le d} a_{ij} x^i y^j. \tag{1}$$

Note that the principal curvatures of $z(x, y)$ will stay as κ_1 and κ_2 regardless of the higher order terms.

To reconstruct a patch surrounding p, we intend to fit the form (1) over tactile data. Fitting is facilitated with the choice of the Darboux frame under which the coefficients of all subcubic terms are known. The tactile data are specially arranged so we can estimate the principal curvatures and locate the principal directions.

B. Solution of Principal Curvatures

We estimate the two principal curvatures κ_1 and κ_2 at the reference point p from normal curvatures in different tangent directions. The angle θ between one of these tangents and one principal direction also determines the other principal direction due to their orthogonality in the tangent plane. So there are essentially three unknowns: $\theta, \kappa_1, \kappa_2$. This suggests that we need to measure at least three normal curvatures, say, $\kappa_\alpha, \kappa_\beta$, and κ_γ in the tangent directions $\boldsymbol{t}_\alpha, \boldsymbol{t}_\beta$, and $\boldsymbol{t}_\gamma$ (shown in Fig. 1), respectively. How to measure these curvatures will be described in Section III-C.

The two principal directions are $\boldsymbol{d}_1$ and $\boldsymbol{d}_2$. The angle θ is from $\boldsymbol{d}_1$ to $\boldsymbol{t}_\alpha$, while the angles θ_1 and θ_2 are from $\boldsymbol{t}_\alpha$ to $\boldsymbol{t}_\beta$ and $\boldsymbol{t}_\gamma$, respectively. Here θ_1 and θ_2 are easily determined from the tangents. The normal curvatures can be expressed in terms of the two principal curvatures [41, p. 137]

$$\begin{aligned} \kappa_\alpha &= \kappa_1 \cos^2 \theta + \kappa_2 \sin^2 \theta \\ \kappa_\beta &= \kappa_1 \cos^2(\theta + \theta_1) + \kappa_2 \sin^2(\theta + \theta_1) \\ \kappa_\gamma &= \kappa_1 \cos^2(\theta + \theta_2) + \kappa_2 \sin^2(\theta + \theta_2). \end{aligned} \tag{2}$$

From (2), we obtain

$$\kappa_\alpha - \kappa_\beta = (\cos(2\theta) - \cos(2\theta + 2\theta_1)) \cdot \frac{\kappa_1 - \kappa_2}{2} \tag{3}$$

$$\kappa_\alpha - \kappa_\gamma = (\cos(2\theta) - \cos(2\theta + 2\theta_2)) \cdot \frac{\kappa_1 - \kappa_2}{2}. \tag{4}$$

In the special case that $\kappa_\alpha = \kappa_\beta = \kappa_\gamma$, two possibilities arise.
   a) $\kappa_1 = \kappa_2$. So, the reference point p is umbilic with constant normal curvature. Every direction in the tangent plane is a principal direction. We arbitrarily choose two orthogonal directions as $\boldsymbol{d}_1$ and $\boldsymbol{d}_2$.
   b) $\kappa_1 \ne \kappa_2$. So, $\cos(2\theta) = \cos(2\theta + 2\theta_1) = \cos(2\theta + 2\theta_2)$, which implies $\theta_1 = \pi, \theta_2 = \pi$, or $\theta_1 - \theta_2 = 0$ or π, namely $\boldsymbol{t}_\alpha = -\boldsymbol{t}_\beta, \boldsymbol{t}_\alpha = -\boldsymbol{t}_\gamma$, or $\boldsymbol{t}_\beta = \pm \boldsymbol{t}_\gamma$. This situation can be avoided by measuring normal curvatures in noncollinear directions.
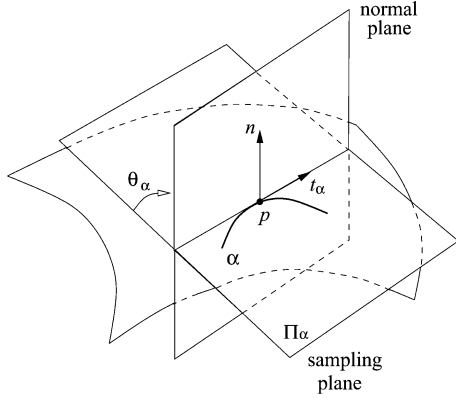
Fig. 2. Data curve α lies where the sampling plane Π_α intersects the surface.

In the general case where κ_α, κ_β, and κ_γ are not all equal, one of the curvatures must be different from the other two. Assume that it is κ_α. A few more steps of manipulation on (3) and (4) yield

$$\tan(2\theta + \theta_2) = \frac{\sin(\theta_1 - \theta_2)}{\frac{\kappa_\alpha - \kappa_\beta}{\kappa_\alpha - \kappa_\gamma} \cdot \frac{\sin\theta_2}{\sin\theta_1} - \cos(\theta_1 - \theta_2)}$$

from which we obtain θ and thus the principal directions. The Darboux frame is now determined. Substituting θ, θ_1, and θ_2 into two of the equations in the system (2), we can solve for the principal curvatures κ_1 and κ_2.

Chen and Schmidt [11] used least-squares fitting over more than three normal curvatures estimated less accurately. The method by Taubin [47], though more robust than ours, requires dense range data.

C. Normal Curvature Estimation

It is time to look at how to determine the tangent plane and measure three normal curvatures at the reference point p. We use a touch sensor to track the surface, while constraining the sensor motion in a plane through p, which we call the *sampling plane*. This is a planar contour tracking problem except the plane is arbitrarily oriented rather than horizontal as studied by many researchers [14], [15], [26], [32]. The tracking data are discrete points along the intersection curve α of the sampling plane and the surface (see Fig. 2). The description of α is, of course, unknown just like the shape. For convenience, we identify these data points with the curve and called them the *data curve*. Then, we fit a quadratic polynomial over those data points very close to p to estimate the tangent, say, $\boldsymbol{t}_\alpha$ and the curvature κ'_α at the point.

Similarly, two other data curves β and γ through p lying in different sampling planes are obtained. We again estimate the tangents $\boldsymbol{t}_\beta$ and $\boldsymbol{t}_\gamma$ as well as the curvatures κ'_β and κ'_γ.

The surface normal $\boldsymbol{n}$ at p is obtained through optimization

$$\min_{\|\boldsymbol{n}\|=1} (\boldsymbol{n} \cdot \boldsymbol{t}_\alpha)^2 + (\boldsymbol{n} \cdot \boldsymbol{t}_\beta)^2 + (\boldsymbol{n} \cdot \boldsymbol{t}_\gamma)^2.$$

With $\boldsymbol{n}$ known, the tangent plane Π at p is determined.

The vectors $\boldsymbol{t}_\alpha$ and $\boldsymbol{n}$ define a normal plane through p that forms an angle θ_α with the sampling plane Π_α. By a result from differential geometry [4, pp. 127–128], the normal curvature in the direction $\boldsymbol{t}_\alpha$ is $\kappa_\alpha = \kappa'_\alpha \cos\theta_\alpha$. Similarly, we obtain the normal curvatures κ_β and κ_γ in the directions $\boldsymbol{t}_\beta$ and $\boldsymbol{t}_\gamma$, respectively.

IV. SURFACE PATCH RECONSTRUCTION

In the Darboux frame formed by the principal directions $\boldsymbol{d}_1$ and $\boldsymbol{d}_2$ and the outward normal $\boldsymbol{n}$, we fit the polynomial description (1) over all the data points (x_i, y_i, z_i), $1 \le i \le n$, sampled along α,

Fig. 3. (a) Broken plastic bottle and (b) its reconstructed neck region by fitting under no constraint.

β, and γ. The degree d of the polynomial is set to be 4.[4] Write $\boldsymbol{a} = (a_{30}, a_{21}, \ldots, a_{04})$ to include the nine polynomial coefficients, which are determined in a least-squares sense

$$\min_{\boldsymbol{a}} f(\boldsymbol{a}) \quad \text{where} \quad f(\boldsymbol{a}) = \frac{1}{n} \sum_{k=1}^{n} (z(x_k, y_k) - z_k)^2. \quad (5)$$

Here, $f(\boldsymbol{a})$ bounds the total squared distance from the data points to the patch (1) defined by $\boldsymbol{a}$.

Fig. 3 shows a broken plastic bottle (a) and the reconstructed patch (b) of the marked neck region. We have sampled $n = 57$ points (red) along three concurrent curves inside the neck region. They are displayed in part (b) of the figure. Their intersection point [marked inside the neck region in part (a)] is parabolic with estimated principal curvatures -0.0423 and 0.0172. We measure the *average fitting error*

$$E = \frac{1}{n} \sum_{k=1}^{n} |z(x_k, y_k) - z_k|. \quad (6)$$

Although the error is small (0.0461 mm) over the 57 data points, the reconstructed patch does not nearly resemble the bottle's neck region. It has "peaks" and "valleys." To get a sense of this discrepancy quantitatively, we use 171 points (blue) sampled along nine extra curves through the same reference point. The average error (6) over these points then rises up dramatically to 13.0041 mm.

A. Constraining the Fitting Surface

Naturally, we would like the reconstructed patch to look "smooth". This patch is assumed to be a "local" one where any drastic changes of geometry like "peaks" or "valleys" between the three data curves are not expected. From the bottle example, it is apparent that three data curves do not provide enough constraints on fitting.

One approach is to generate artificial data points by, say, interpolation, between the data curves, and then fit over all the data. After many trials, we have found that interpolation simply could not produce satisfactory shapes when verified against extra real data. Artificial data points tend to shape the surface fit with a bias imposed by the interpolation scheme itself. The areas between the three data curves are just too large for interpolation using some spline-like functions.

The objective function in (5) for fitting needs to include a term that can measure the "degree of folding" of the surface fit. We make use of the *total Gaussian curvature*, which is defined as the integral of the Gaussian curvature over a surface patch $\sigma : \iint_\sigma K \, dA$. Geometrically, it is the algebraic area of the region formed by points on the unit sphere that correspond to all normals on the patch [39, p. 290].

---

[4]Quartic polynomials are capable of describing a wide range of real objects so that several subclasses are commonly used as shape models.

Let D be the domain of the surface fit in the tangent plane at the reference point p (i.e., the xy-plane). Since a patch may be "folded" many times over a small region on the unit sphere to still yield a small total Gaussian curvature, we use the absolute value of K:[5]

$$\iint_D |K(x, y)| \cdot \sqrt{1 + z_x^2 + z_y^2}\, dx dy. \qquad (7)$$

Here, the area element $\sqrt{1 + z_x^2 + z_y^2}\, dx dy$ is included. The more the patch folds, the larger the integral (7), and *vice versa*. The reconstructed patch in Fig. 3 has total absolute Gaussian curvature 16.6031, which is too big[6] for a small region on the bottle.

Given a polynomial surface fit (1) with the coefficient vector $\boldsymbol{a}$, we evaluate the total absolute Gaussian curvature (7) numerically. For the ease of computation, the patch domain D is chosen to be inside a cubic spline that passes through the end points of the projections of α, β, and γ onto the xy-plane. Discretize D into a grid of m points $(u_1, v_1), \ldots, (u_m, v_m)$ with uniform spacing h. The integral (7) is approximated by

$$g(\boldsymbol{a}) = h^2 \cdot \sum_{j=1}^{m} \Bigg(|K(u_j, v_j)|$$
$$\cdot \sqrt{1 + z_x^2(u_j, v_j) + z_y^2(u_j, v_j)} \Bigg). \qquad (8)$$

Patch reconstruction over the n data points is done through minimizing the total absolute Gaussian curvature subject to the constraint that the surface fit should "pass through" these points

$$\min_{\boldsymbol{a}} g(\boldsymbol{a}) + \lambda f(\boldsymbol{a}). \qquad (9)$$

The Lagrange multiplier λ has the unit mm^{-2}.

B. Minimization

Note that the function $g(\boldsymbol{a})$ depends on the signs of the Gaussian curvatures $K(u_j, v_j), 1 \leq j \leq m$, which could vary from the current coefficient estimate $\boldsymbol{a}^{(l)}$ to the next one $\boldsymbol{a}^{(l+1)}$. To cope with this issue, at $\boldsymbol{a}^{(l)}$ for every grid point (u_j, v_j), we define

$$\delta_j = \begin{cases} 1 & \text{if } K(u_j, v_j) \geq 0; \\ -1 & \text{if } K(u_j, v_j) < 0. \end{cases}$$

Replace $|K(u_j, v_j)|$ with $\delta_j K(u_j, v_j)$ in the definition (8) of $g(\boldsymbol{a})$. This results in an equivalent function $\tilde{g}(\boldsymbol{a})$ in some neighborhood of $\boldsymbol{a}^{(l)}$ in the coefficient space. Performing the steepest descent along the negative gradient $-\nabla (f(\boldsymbol{a}) + \lambda \tilde{g}(\boldsymbol{a}))$ yields the next estimates $\boldsymbol{a}^{(l+1)}$ and $\lambda^{(l+1)}$. If the gradient becomes zero, we have found a (local) minimum of (9). Otherwise, the iterations continue. The initial value of the coefficient vector, $\boldsymbol{a}^{(0)}$, is obtained from unconstrained fitting of (5) over the data points and some onetime artificial points generated through linear interpolation. The initial value $\lambda^{(0)}$ is chosen after several trials.

We reconstruct the neck region of the plastic bottle in Fig. 3(a)[7] over the same three (red) data curves from Fig. 3(b), and the result is shown in Fig. 4. The same nine extra curves (shown in blue dots) from Fig. 3(b) yield an average fitting error (6) of 0.0859 mm, a dramatic decrease from 13.0041 mm for the old patch generated by fitting under no constraint. The total absolute Gaussian curvature of the new patch is 0.0329

---

[5]Minimization of the total absolute Gaussian curvature for triangulating a dense data set was introduced by van Damme and Alboul [50]. An NP-hardness result was given in [8] for such triangulation of a terrain with fixed vertex set and boundary.

[6]The total curvature of any closed smooth surface in 3-D is only 4π, which equals the area of a unit sphere.

[7]The multiplier λ has value 9.99 mm^{-2}.
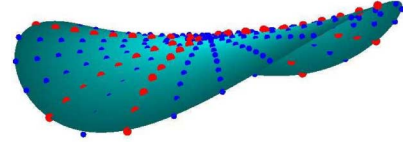
Fig. 4. New patch reconstructed over the same neck region in Fig. 3 by fitting while minimizing the total absolute Gaussian curvature.

(a)   (b)
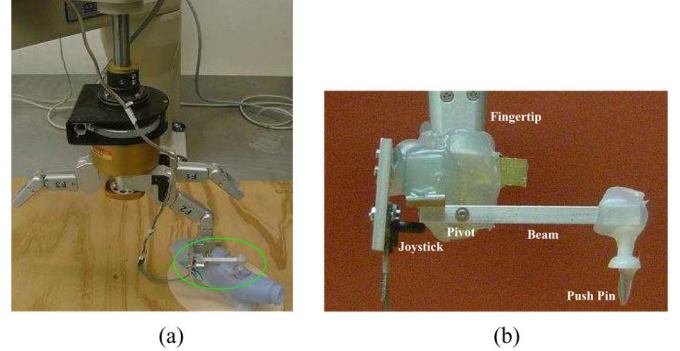
Fig. 5. Setup for surface tracking and reconstruction: (a) Adept manipulator, BarrettHand, and touch mechanism (encircled), which is enlarged in (b).

compared to 16.6031 for the old patch. The slight increase in the average error from 0.0461 to 0.0514 mm over the three original curves is expected because of the extra term $g(\boldsymbol{a})$ in (9) to minimize.

V. Implementation and Reconstruction Results

As shown in Fig. 5, the experimental setup includes an Adept Cobra 600 manipulator, a three-fingered BarrettHand, and a joystick-based tracking device. Here, the joystick[8] is horizontally placed and right below a pivoted lever beam. When a vertical push pin attached to the beam's distant end touches a surface, its close end moves downward, causing the joystick to bend. The contact point between the push pin and the surface can be located using the combined forward kinematics of the Adept's end-effector and the BarrettHand.

The Adept manipulator has four DOFs, same does the BarrettHand. Nevertheless, only one finger is used in the tracking and it does not have yaw. So the push pin has only five DOFs. For convenience of implementation, we limit the tracking motions to be in the vertical planes.

While sampling data points along a curve, the system estimates the current normal direction, and align the orientation of the Joystick sensor with the normal estimate by rotating the corresponding finger of the BarrettHand. The tracking motion is made up of small movements within each of which the robot commands constant horizontal and vertical velocities. The distance of a vertical movement is determined based on the force measurement from the joystick.

To determine the accuracy, we match reconstructed patches on several objects against their mesh models generated by NextEngine's desktop 3-D scanner. The accuracy of the scanner is 0.127 mm. Each mesh model has between 16 000 and 85 000 vertices that form dense point clouds. The normal at a mesh vertex is estimated by averaging the normals of its adjacent triangles. To align a patch with the corresponding mesh model, we place its reference point at a vertex on the model. Align the tangent plane at the vertex with the xy-plane in the local Darboux frame at the reference point, and rotate the data curves about the z-axis to find the best match. Iterating over all the mesh vertices will register the data curves onto the mesh model.

---

[8]With frequency 10–100 Hz and force range of 0.196–1.666 N.

TABLE I
SURFACE PATCHES (BLACK) RECONSTRUCTED SURROUNDING MARKED REFERENCE POINTS ON A SHELL, A WOODEN PEAR, AND A PEBBLE, RESPECTIVELY.
EACH RECONSTRUCTED PATCH IS PRESENTED IN TWO VIEWS: OUTSIDE-IN AND INSIDE-OUT
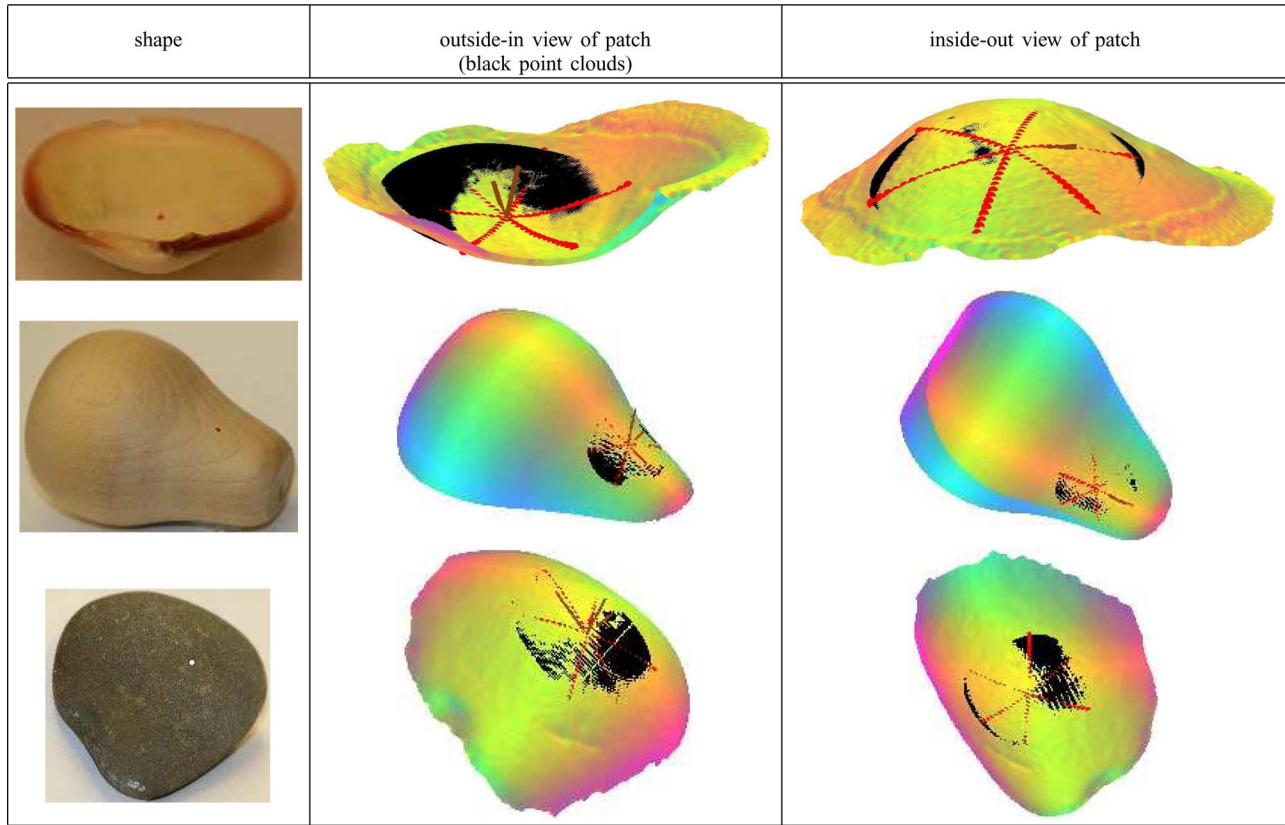
TABLE II
EUCLIDEAN DISTANCES (MILLIMETERS) FROM THE TACTILE DATA POINTS AND THE VERIFYING MESH VERTICES
TO THE PATCHES (LABELED TAGC) SHOWN IN TABLE I AND THOSE RECONSTRUCTED
BY MINIMIZING THE QUADRATIC VARIATION (QV)

shape	tactile data points			mesh vertices in patch area			size ratio of tactile data to testing data	total mesh vertices on the model
		dist. to patch (mm)			dist. to patch (mm)			
	num.	TAGC	QV	num.	TAGC	QV		
shell	97	0.2782	0.2420	5248	0.2283	0.2391	1.85%	19181
pear	63	0.0613	0.0664	1779	0.0991	0.0946	3.54%	84656
dark pebble	81	0.0998	0.1065	4423	0.1308	0.1327	1.83%	16028

With the data curves registered, the mesh vertices that project onto the patch domain[9] are considered "overlapped" with the patch. The minimum Euclidean distances from these overlapped vertices to the patch are averaged. The patch in Fig. 4 is matched against a mesh model of the bottle neck region. The overlapped vertices on the mesh model are at an average Euclidean distance of 0.130 mm from the patch. The actual distance is within 0.257 mm if we take into account the 0.127 mm accuracy of the scanner.

Table I displays patch reconstruction results over three more shapes. [10] The first column in the table lists the three objects with reference points marked for tracking. The second and third columns present two views (from the outside and the inside, respectively) of each reconstructed patch (rendered as black point clouds) overlaid onto the corresponding mesh model.[11] The data curves are shown in red, while the Darboux frame in brown. In each view, only the points in the patch that are not occluded by the mesh model are displayed. Namely, the patch is

the union of the black points from the two views. The color of a vertex on the mesh model is rendered in the RGB space based on the x-, y-, and z-coordinates of its unit outward normal.

Table II compares the three reconstructed patches based on the total absolute Gaussian curvature (TAGC), respectively, with those reconstructed by minimizing the quadratic variation (QV)

$$\iint_D z_{xx}^2 + 2z_{xy}^2 + z_{yy}^2 \, dxdy$$

subject to the data constraint $f(\boldsymbol{a}) = 0$. The above form originates from the strain energy of a (flat) plate with unit Poisson's ratio under small deformations [49, p. 47]. In [22], it is shown to be the optimal functional for surface fitting over sparse data under several conditions including rotational symmetry.

The table lists, for each reconstructed patch, its average (absolute) distances from the tactile data curves and from the overlapped mesh vertices, respectively. The TAGC patches have slightly smaller errors than the QV patches in four out of six comparisons, especially, when the patches are more curved. For each method, the average errors over the tactile data and the mesh vertices differ by hundredths of millimeters

---

[9]approximated by the region inside a closed cubic spline through the projections of the endpoints of the athree data curves onto the tangent plane.

[10]On average, tracking took 5 to 10 min while fitting took 10 min.

[11]For display purpose, the mesh models are not shown in their entirety.

only, despite that the number of data points used in the patch reconstruction is at most 3.54% of that of mesh vertices used in verification. Even if we take into account the 0.127 mm accuracy of the scanner, this error difference is still within 0.18 mm for each patch.

VI. Discussion

This paper investigates how to reconstruct patches on curved objects from tactile data curves generated by robot finger tracking. Such a situation arises in a task that involves close interactions between a robot hand and an object, and where a camera or range sensor becomes ineffective due to occlusions. Potential applications are tasks from grasping and dexterous manipulation of objects with unknown geometry to robot-assisted surgery to robot climbing.

Another objective of our work is to understand the *minimum* amount of tactile data sufficient for approximating a surface, or at least a patch. We intend to use only "1-D" tactile data for patch reconstruction. Existing reconstruction algorithms require data points, whether range or tactile, dense or sparse, to be 2-D arrays or "clouds." The minimization of Gaussian curvature while fitting can be viewed as a regularization technique [40] for solving the ill-posed problem of surface reconstruction. Superquadric or B-spline surfaces such as NURBS are powerful representations. However, these techniques are not expected to work well on "1-D" data, as implied by Fig. 3(b).

Several factors affect the size of the reconstructed patch: curvatures in the reconstructed region and the limit by the fitting form (1). A higher degree polynomial is expected to describe a high-curvature surface region better, and in general, a larger one as well. More robust tracking control is needed to maintain data accuracy, The data curves sampled from the surface do not need to be planar. Even though the objects in our experiment are immobilized, the reconstruction method can be incorporated into dexterous manipulation, especially under rolling contact [4], [13], which allow the mapping of tactile data acquired at different time instants into the same frame.

Probing the surface at a grid of points could possibly lead to a more robust fitting result or a larger patch area than tracking along three concurrent curves. However, multiple mechanical probes are time consuming because the robot hand needs to move up and down repeatedly. Curve tracking is much more efficient, and it mimics the human fingers moving across a surface to feel its shape.

A coordinate-measuring machine (CMM) can achieve an accuracy of tenths of a micron. However, it is almost impossible to integrate its colossal closed-frame structure with a robot hand.

A complicated surface can be represented as a graph, where every node corresponds to one local patch on the surface and every edge corresponds to the boundary curve between two adjacent patches. Each patch is described in its local frame that best reflects its geometry. Fitting will be subject to constraints such as smoothness, tangential continuity, and concentricity [7], [44]. Automated selection of reference points need to be implemented to partition the surface into patches that reflect its topology. A better approach of obtaining global geometry, perhaps, is to combine tracking-based reconstruction with a technique based on vision [1] or range sensing.

Acknowledgment

References

[1] P. K. Allen, "Integrating vision and touch for object recognition tasks," *Int. J. Robot. Res.*, vol. 7, pp. 15–33, Aug. 1988.

[2] P. K. Allen and P. Michelman, "Acquisition and interpretation of 3-D sensor data from touch," *IEEE Trans. Robot. Autom.*, vol. 6, pp. 397–404, Aug. 1990.

[3] J. Baeten and J. De Schutter, "Hybrid vision/force control at corners in planar robotic-contour following," *IEEE/ASME Trans. Mechatron.*, vol. 7, pp. 143–151, Apr. 2002.

[4] A. Bicchi, A. Marigo, and D. Prattichizzo, "Dexterity through rolling: Manipulation of unknown objects," in *Proc. IEEE Int. Conf. Robot. Autom.*, 1999, pp. 1583–1588.

[5] M. M. Blane, Z. Lei, H. Çivi, and D. B. Cooper, "The 3L algorithm for fitting implicit polynomial curves and surfaces to data," *IEEE Trans. Pattern Anal. Mach. Intell.*, vol. 22, pp. 298–313, Mar. 2000.

[6] J.-D. Boissonnat, "Geometric structure for three-dimensional shape representation," *ACM Trans. Graphics*, vol. 3, pp. 266–286, Oct. 1984.

[7] R. M. Bolle and B. C. Vemuri, "On three-dimensional surface reconstruction methods," *IEEE Trans. Pattern Anal. Mach. Intell.*, vol. 13, pp. 1–13, Jan. 1991.

[8] M. Buchin and J. Giesen, "Minimizing the total absolute Gaussian curvature in a terrain is hard," in *Proc. Can. Conf. Comp. Geometry*, 2005, pp. 192–195.

[9] M. Charlebois, K. Gupta, and S. Payandeh, "Shape description of curved surfaces from contact sensing using surface normals," *Int. J. Robot. Res.*, vol. 18, pp. 779–787, Aug. 1999.

[10] N. Chen, R. Rink, and H. Zhang, "Local object shape from tactile sensing," in *Proc. IEEE Int. Conf. Robot. Autom.*, 1996, pp. 3496–3501.

[11] X. Chen and F. Schmitt, "Intrinsic surface properties from surface triangulation," in *Proc. Eur. Conf. Comp. Vision*, 1992, pp. 739–743.

[12] K. K. Choi, S. L. Jiang, and Z. Li, "Multifingered robotic hands: Contact experiments using tactile sensors," in *Proc. IEEE Int. Conf. Robot. Autom.*, 1998, pp. 2268–2273.

[13] A. A. Cole, J. E. Hauser, and S. S. Sastry, "Kinematics and control of multifingered hands with rolling contact," *IEEE Trans. Autom. Contr.*, vol. 34, pp. 298–404, Apr. 1989.

[14] S. Demey, H. Bruyninckx, and J. De Schutter, "Model-based planar contour following in the presence of pose and model errors," *Int. J. Robot. Res.*, vol. 16, pp. 840–858, Dec. 1997.

[15] J. De Schutter and H. Van Brussel, "Compliant robot motion I and II," *Int. J. Robot. Res.*, vol. 7, pp. 3–33, Aug. 1988.

[16] G. Dudek and J. K. Tsotsos, "Recognizing planar curves using curvature-tuned smoothing," in *Proc. IEEE Int. Conf. Pattern Recogn.*, 1990, pp. 130–135.

[17] R. E. Ellis and M. Qin, "Singular-value and finite-element analysis of tactile shape recognition," in *Proc. IEEE Int. Conf. Robotics Automation*, 1994, pp. 2529–2535.

[18] R. S. Fearing, S. T. Venkataraman and T. Iberall, Eds., "Tactile sensing for shape interpretation," *Dextrous Robot Hands*, pp. 209–238, 1990.

[19] R. S. Fearing and T. O. Binford, "Using a cylindrical tactile sensor for determining curvature," in *Proc. IEEE Int. Conf. Robot.*, 1988, pp. 765–771.

[20] F. P. Ferrie, J. Lagarde, and P. Whaite, "Darboux frames, snakes, and super-quadrics: Geometry from the bottom up," *IEEE Trans. Pattern Anal. Mach. Intell.*, vol. 15, pp. 771–784, Aug. 1993.

[21] P. J. Flynn and A. K. Jain, "On reliable curvature estimation," in *Proc. IEEE Conf. Computer Vision Pattern Recog.*, 1989, pp. 110–116.

[22] W. E. L. Grimson, "A computational theory of visual surface interpolation," *Philosoph. Trans. R. Soc. London B*, vol. 298, pp. 395–427, Sep. 1982.

[23] E. Hameiri and I. Shimshoni, "Estimating the principal curvatures and the Darboux frame from real 3-D range data," *IEEE Trans. Syst. Man. Cybern.*, vol. 33, pt. B, pp. 626–637, Aug. 2003.

[24] R. D. Howe and M. R. Cutkosky, "Dynamic tactile sensing: Perception of fine surface features with stress rate sensing," *IEEE Trans. Robot. Automat.*, vol. 9, pp. 140–151, Apr. 1993.

[25] R. Ibrayev and Y.-B. Jia, "Semi-differential invariants for tactile recognition of algebraic curves," *Int. J. Robot. Res.*, vol. 24, pp. 951–969, Nov. 2005.

[26] F. Jatta, G. Legnani, and A. Visioli, "Hybrid force/velocity control of industrial manipulators with elastic transmissions," in *Proc. IEEE/RSJ Int. Conf. Intell. Robots. Syst.*, 2003, pp. 3276–3281.

[27] Y.-B. Jia, L. Mi, and J. Tian, "Surface patch reconstruction via curve sampling," in *Proc. IEEE Int. Conf. Robot.*, 2006, pp. 1371–1377.

[28] D. Keren, D. Cooper, and J. Subrahmonia, "Describing complicated objects by implicit polynomials," *IEEE Trans. Pattern Anal. Mach. Intell.*, vol. 16, pp. 38–53, Jan. 1994.

[29] D. Keren and C. Gotsman, "Fitting curves and surfaces with constrained implicit polynomials," *IEEE Trans. Pattern Anal. Mach. Intell.*, vol. 21, pp. 31–41, Jan. 1999.

[30] D. Keren, E. Rivlin, and I. Shimshoni, "Recognizing 3D objects using tactile sensing and curve invariants," *J. Math. Imag. Vis.*, vol. 12, pp. 5–23, Jan. 2000.

[31] O. Khatib and J. Burdick, "Motion and force control of robot manipulators," in *Proc. IEEE Int. Conf. Robot.*, 1986, pp. 1381–1386.

[32] F. Lange and G. Hirzinger, "Learning force control with position controlled robots," in *Proc. IEEE Int. Conf. Robot.*, 1996, pp. 2282–2288.

[33] C. Lin and M. J. Perry, "Shape description using surface triangulation," in *Proc. IEEE Workshop Comp. Vision*, 1982, pp. 38–43.

[34] D. Meyers and S. Skinner, "Surfaces from contours," *ACM Trans. Graph.*, vol. 11, pp. 228–258, Jul. 1992.

[35] L. Mi and Y.-B. Jia, "High precision contour tracking with a joystick sensor," in *Proc. IEEE/RSJ Int. Conf. Intell. Robot. Syst.*, 2004, pp. 804–809.

[36] M. Moll and M. A. Erdmann, , J.-D. Boissonnat, J. Burdick, K. Goldberg, and S. Hutchinson, Eds., "Reconstructing the shape and motion of unknown objects with active tactile sensors," in *Algorithmic Foundations of Robotics V*. Berlin, Germany: Springer-Verlag, 2004, pp. 293–309.

[37] D. J. Montana, "The kinematics of contact and grasp," *Int. J. Robot. Res.*, vol. 7, pp. 17–32, Jun. 1988.

[38] A. M. Okamura, N. Smaby, and M. R. Cutkosky, "An overview of dexterous manipulation," in *Proc. IEEE Int. Conf. Robotics*, 2000, pp. 255–262.

[39] B. O'Neill, *Elementary Differential Geometry*. New York: Academic, 1966.

[40] T. Poggio, V. Torre, and C. Koch, "Computational vision and regularization theory," *Nature*, vol. 317, pp. 314–319, 1985.

[41] A. Pressley, *Elementary Differential Geometry*. Berlin, Germany: Springer-Verlag, 2001.

[42] M. H. Raibert and J. J. Craig, "Hybrid position/force control of manipulators," *J. Dyn. Syst. Meas. Contr.*, vol. 102, pp. 126–133, 1981.

[43] R. A. Russell and S. Parkinson, "Sensing surface shape by touch," in *Proc. IEEE Int. Conf. Robot.*, 1993, pp. 423–428.

[44] B. Sarkar and C.-H. Menq, "Smooth-surface approximation and reverse engineering," *Comput.-Aided Des.*, vol. 23, pp. 623–628, Nov. 1991.

[45] E. M. Stokely and S. Y. Wu, "Surface parameterization and curvature measurement of arbitrary 3-D objects: Five practical methods," *IEEE Trans. Pattern Anal. Mach. Intell.*, vol. 14, pp. 833–840, Aug. 1992.

[46] S. Sullivan, L. Sandford, and J. Ponce, "Using geometric distance fits for 3-D object modeling and recognition," *IEEE Trans. Pattern Anal. Mach. Intell.*, vol. 16, pp. 1183–1196, Dec. 1994.

[47] G. Taubin, "Estimating the tensor of curvature of a surface from a polyhedral approximation," in *Proc. IEEE Int. Conf. Comp. Vision*, 1995, pp. 902–907.

[48] G. Taubin, F. Cukierman, S. Sullivan, J. Ponce, and D. J. Kriegman, "Parameterized families of polynomials for bounded algebraic curve and surface fitting," *IEEE Trans. Pattern Anal. Mach. Intell.*, vol. 16, pp. 287–303, Mar. 1994.

[49] S. P. Timoshenko and S. Woinowsky-Krieger, *Theory of Plates and Shells*, 2nd ed. New York: McGraw-Hill, 1959.

[50] R. van Damme and L. Alboul, , M. Dæhlen, T. Lyche, and L. L. Schumaker, Eds., "Tight triangulations," in *Mathematical Methods for Curves and Surfaces*. Nashville, TN: Vanderbilt Univ. Press, 1995, pp. 517–526.

[51] D. Xiao, B. K. Ghosh, N. Xi, and T. J. Tarn, "Sensor-based hybrid position/force control of a robot manipulator in an uncalibrated environment," *IEEE Trans. Contr. Syst. Technol.*, vol. 8, pp. 635–645, Jul. 2000.

Orchestration of Grid-Enabled Geospatial Web Services in Geoscientific Workflows

Gobe Hobona, *Member, IEEE*, David Fairbairn, Hugo Hiden, and Philip James

Abstract—The need for computational resources capable of processing geospatial data has accelerated the uptake of geospatial web services. Several academic and commercial organizations now offer geospatial web services for data provision, coordinate transformation, geocoding and several other tasks. These web services adopt specifications developed by the Open Geospatial Consortium (OGC)—the leading standardization body for Geographic Information Systems. In parallel with efforts of the OGC, the Grid computing community has published specifications for developing Grid applications. The Open Grid Forum (OGF) is the main body that promotes interoperability between Grid computing systems. This study examines the integration of Grid services and geospatial web services into workflows for Geoscientific processing. An architecture is proposed that bridges web services based on the abstract geospatial architecture (ISO19119) and the Open Grid Services Architecture (OGSA). The paper presents a workflow management system, called SAW-GEO, that supports orchestration of Grid-enabled geospatial web services. An implementation of SAW-GEO is presented, based on both the Simple Conceptual Unified Flow Language (SCUFL) and the Business Process Execution Language for Web Services (WS-BPEL or BPEL for short).

Note to Practitioners—Geoscientific workflows are used in several disciplines including for example geology, geophysics hydrology, and petroleum science. Some of the analysis carried out by geoscientists can now be offered on the World Wide Web using standardized web services. Our study examines the potential of workflow enactors to support the creation of geoscientific workflows involving web services based on standards of the Open Geospatial Consortium. An implementation of a prototype is presented and applied to the analysis of groundwater vulnerability using borehole data. A sample workflow is implemented using two different workflow enactors and their distinct languages to demonstrate that the proposed approach is independent of the workflow enactor adopted. The proposed approach could be used to support collaborative workflows that involve analytical services provided by multiple organizations

Index Terms—Automation, geographic information systems, geology, geophysics.

I. INTRODUCTION

Geoscientists use Geographic Information Systems (GIS) in almost all their data management, processing, and analytical activities. The development of standards for geospatial interoperability between GIS is spearheaded by the Open Geospatial Consortium (OGC)—a

G. Hobona is with the Centre for Geospatial Science (CGS), University of Nottingham, Nottingham, NG7 2RD, U.K. (e-mail: gobe. hobona@nottingham.ac.uk).

D. Fairbairn and P. James are with the School of Civil Engineering and Geosciences, Newcastle University, Newcastle upon Tyne, NE1 7RU, U.K. (e-mail: dave.fairbairn@newcastle.ac.uk; philip.james@newcastle.ac.uk).

H. Hiden is with the North East Regional e-Science Centre (NEReSC), School of Computing Science, Newcastle University, Newcastle upon Tyne, NE 1 7RU, U.K. (e-mail: h.g.hiden@newcastle.ac.uk).

Color versions of one or more of the figures in this paper are available online at http://ieeexplore.ieee.org.